

# Entanglement-assisted Hamiltonian dynamics learning

Ayaka Usui,<sup>1,\*</sup> Guillermo Abad-López,<sup>1,2,†</sup> Hari Krishnan  
SV,<sup>1,‡</sup> Anna Sanpera,<sup>1,3,§</sup> and Some Sankar Bhattacharya<sup>1,¶</sup>

<sup>1</sup>*Física Teòrica: Informació i Fenòmens Quàntics, Departament de Física,  
Universitat Autònoma de Barcelona, 08193 Bellaterra, Spain*

<sup>2</sup>*Qilimanjaro Quantum Tech, Carrer de Veneçuela 74, 08019, Barcelona, Spain*

<sup>3</sup>*ICREA, Pg. Lluís Companys 23, 08010 Barcelona, Spain*

Approximating the dynamics given by a complex many-body Hamiltonian with a simpler effective model lies at the interface of quantum Hamiltonian learning and quantum simulation. In this context, quantum generative adversarial networks (QGANs) have been shown to outperform standard Trotter-based approximations. However, their performance is often hindered by training plateaus and local minima that become increasingly severe with system size. To overcome these limitations, we propose an entanglement-assisted learning strategy that couples a single randomly initialized auxiliary qubit to the learning system at an intermediate stage of the training process. The interplay between randomization and entanglement significantly enhances the learning performance of the protocol.

*Introduction.*— The properties of quantum many-body systems are intimately linked to the operator content of the Hamiltonian that governs their dynamics [1]. Given incomplete data originating from an unknown Hamiltonian, quantum Hamiltonian learning (QHL) encompasses a variety of methods aimed at inferring its operator structure, i.e., type of interactions and their strengths [2–14]. Such data may stem from experimental limitations such as restricted access to expectation values of certain observables, or from theoretical constraints, for instance, having access to only a single eigenvector of the so-called parent Hamiltonian [15]. Quantum simulators, on the other hand, are purpose-built experimental platforms, either analog or digital, designed to probe and extract properties of complex quantum systems that are intractable for classical computation [16–20]. These two approaches, QHL and quantum simulation, can be viewed as dual tasks: one seeks to reconstruct a parent Hamiltonian from restricted data, while the other generates data from non-trivial Hamiltonians to infer properties of complex many-body quantum systems.

Between these two paradigms lies the task of Hamiltonian approximation, replacing a complex, possibly unknown Hamiltonian with a simpler, experimentally feasible one [21, 22]. This goal is relevant to both QHL and quantum simulation, as it enables tractable modeling and experimental realization of otherwise inaccessible quantum systems. A representative example involves approximating highly non-local Hamiltonians—such as those arising, for instance, in lattice gauge theories with three- or four-body interactions—by simpler Hamiltonians involving only two and one-body interactions. More generally, given an unknown complex target Hamiltonian

$H_T$  of locality  $k$ , one may ask: What is the best approximation of its dynamics? Meaning what is the optimal effective Hamiltonian we can generate,  $H_G$ , composed only of one- and two-body interactions, that reproduces the same unitary evolution [22].

Generically, the unitary evolution of non-trivial Hamiltonians,  $U_T = e^{-iH_T t}$ , involves computing the exponential of a sum of non-commuting operators. This is usually approached using the Trotter decomposition, which approximates the total time evolution into very short time steps and breaks the exponential of the sum into a product of simpler exponentials. In digital quantum computation, the Trotter approximation can be implemented as a sequence of one- and two-qubit gates [17]. If the sequence of gates is sufficiently long, the approximation converges to the exact unitary evolution. However, the Trotter decomposition does not necessarily yield the most efficient gate sequence to simulate the dynamics. To address this limitation, various alternative techniques have been proposed, see for instance [23].

Here we employ quantum generative adversarial networks (QGANs), an unsupervised quantum machine learning model proposed in [24, 25], as a quantum extension of its successful classical counterpart; generative adversarial networks [26]. The learning efficiency of QGANs has been reported in multiple instances for both quantum and classical data [27–33]. An example of such efficiency for learning Hamiltonian unitary evolution was provided in [34], where for a fixed time, the unitary evolution of a 3-qubit Heisenberg Hamiltonian evolution requires  $\sim 10^4$  gates using the Trotter approximation, whereas the QGAN implementation achieved the same high-fidelity with just 52 gates.

Nevertheless, as in many machine learning protocols involving the minimization of a cost function in a large phase space, optimization of the training algorithm is hindered by unstable convergence and the vanishing gradient of the cost function [35]. As a consequence, the training may exhibit stagnation, even when sufficient resources are allocated in the QGAN. For example, increas-

\* [ayaka.usui@uab.cat](mailto:ayaka.usui@uab.cat)

† [guillermo.abad@uab.cat](mailto:guillermo.abad@uab.cat)

‡ [hari Krishnan.sasidharan@uab.cat](mailto:hari Krishnan.sasidharan@uab.cat)

§ [anna.sanpera@uab.cat](mailto:anna.sanpera@uab.cat)

¶ [somesankar.bhattacharya@uab.cat](mailto:somesankar.bhattacharya@uab.cat)

ing the number of gates may increase the expressivity of the algorithm and improve the probability of a successful optimisation; however, redundant gates can also stagnate the training, and even if the training goes well, it results in a lengthier final decomposition.

In this work, we address the above challenges and propose an efficient strategy for learning unitaries within the QGAN framework. Our goal is twofold. First, we aim to approximate the dynamics of an unknown complex Hamiltonian with a simpler one that contains only the minimal number of one-body and two-body terms. Second, we show that incorporating an ancillary system during the training phase helps mitigate stagnation, effectively leveraging entanglement to facilitate the learning process. In doing so, our method not only enhances the overall efficiency of QGAN training but also enables a more compact decomposition of the target unitary transformation. Before proceeding further, we briefly review the fundamentals of QGANs.

*Unitary learning via QGANs.*— A learning process for both, classical and quantum states, can be formulated as an adversarial game between two players: a generator  $G$  and a discriminator  $D$ , trying to learn an unknown state  $T$ . The generator's goal is to produce states that resemble, as closely as possible, the target  $T$ , while the discriminator seeks to distinguish them using a cost function,  $\mathcal{L}$ , which quantifies their distance. To all effects, the target  $T$  can be treated as a black box.

During the learning process, both the generator and the discriminator are updated alternately. First, with the discriminator fixed, the generator parameters  $G(\theta)$  are adjusted to approach the target state, minimizing the cost function. Then, given the just-found, closer generated state, the discriminator  $D(\phi)$  is improved, maximizing the cost function. This adversarial interaction can be naturally framed as a minimax game:  $\min_{\theta} \max_{\phi} \mathcal{L}(\psi_T, \psi_{G(\theta)}, D(\phi))$ , where the improvement of one component drives the refinement of the other, allowing for unsupervised learning of states.

Assuming that both the generator and discriminator have infinite capacity, the optimization landscape can be chosen convex [24], with the training eventually reaching its Nash equilibrium. There, the generator state is identical to the target, and the discriminator cannot tell them apart. Therefore, while in general the cost function both increases and decreases during training due to the two opposing optimizations, the adversarial learning finishes by maximizing the fidelity between the generated and target states.

A quantum circuit architecture is typically employed to implement QGANs (optimal control methods can also be used [36]). With the generator consisting of a parametrized quantum circuit, constructed with multiple layers of parametrized gates, as schematically depicted in Fig. 1(b), and the discriminator framed as a parametrized operator that differentiates the target state and the generator state, with such differentiation depending on the

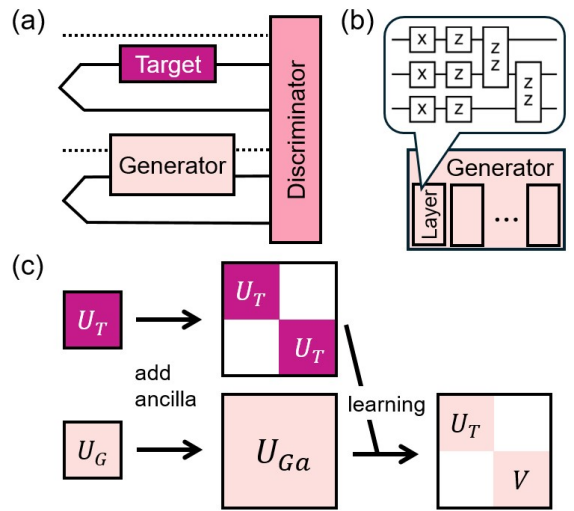


FIG. 1. (a) Layout of ancilla-assisted QGANs. The auxiliary ancilla (dotted line) is embedded in the generator  $G$ . The input state is given by Eq. (3). (b) The generator is composed of several layers, with each layer consisting of single-qubit rotations  $X$ ,  $Z$ , and two-qubit interactions  $ZZ$ . (c) Sketch of ancilla-assisted learning, where  $U_T$ ,  $U_G$ , and  $U_{Ga}$  are, respectively, the operators of the target, the original generator, and the ancilla-expanded generator, with  $V$  a new redundancy not used for training. The white areas indicate zeros. The expanded  $U_{Ga}$  is trained against a block diagonal target until the top-left generator subspace approximates the target.

cost function. In this work, we use the quantum Wasserstein distance [34, 37, 38], as the cost function. This metric is a continuous analog of the quantum "Hamming distance", allowing for a smooth optimisation over multiple qubits. It contrasts with other metrics such as, e.g., the trace distance, which usually decay exponentially with increasing number of qubits.

At the cost of increasing the number of input qubits, QGANs can be designed for the learning of unitaries by exploiting Choi-Jamiołkowski isomorphism [39, 40], where rather than replicating  $U_T$  by sending batches of multiple different states to both the target and the generator [41], a maximally entangled state  $|\Omega\rangle$  is used [34, 36]. Assuming that the target acts on an  $N$ -qubit system, one prepares, as input, a maximally entangled  $2N$ -qubit state of the form:

$$|\Omega\rangle = \frac{1}{\sqrt{d}} \sum_{i=0}^{d-1} |i\rangle_A |i\rangle_B, \quad (1)$$

where  $d = 2^N$  is the dimension of the Hilbert space, while  $|i\rangle_{A(B)}$  denotes a state of the computational basis of  $N$ -qubits of system A(B). Such a configuration is symbolically sketched by solid lines in Fig. 1(a).

The fidelity between the output states of the target unitary,  $U_T$ , and those of the generator,  $U_G$ , when both

act only in one half of the system (B), is given by:

$$F = \left| \langle \Omega | (\mathbb{I}_A \otimes U_G)^\dagger (\mathbb{I}_A \otimes U_T) | \Omega \rangle \right|^2 = \frac{1}{d^2} \left| \text{Tr}[U_G^\dagger U_T] \right|^2, \quad (2)$$

which is proportional to the Hilbert-Schmidt inner product of the operators  $\langle U_G U_T \rangle = \text{Tr}(U_G^\dagger U_T)$ . The fidelity reaches its maximum value,  $F = 1$ , if and only if  $U_G$  and  $U_T$  differ at most by a global phase. Thus, training takes the generator towards  $U_G \simeq U_T$ , despite  $H_G \neq H_T$ .

*Ancilla-assisted learning.*— The QGAN learning process can be framed as an optimization process that aims to provide the best approximation to  $U_T$  within a fixed set of resources. Those involve the number of layers in  $G$ , the number of gates on each layer, the number of iterations, and the total time evolution. Typically, the central question is determining which generator ansatz and how many layers are required to achieve a sufficiently close approximation to the target, given a fixed number of training iterations. In practice, however, it is not always possible to find the optimal decomposition of  $U_T$  within a reasonable training effort (number of iterations), due to QGANs facing several variational circuits pathologies, like most quantum machine learning protocols do [42, 43]. Due to restricted capacities, redundant gates, and finite training times, optimization landscapes exhibit learning plateaus or local minima, creating unfavourable initial points for which the fidelity saturates at values much below one, or do not even converge to any given value.

To address the above issue, we increase the generator phase space by adding an *interacting ancillary qubit*. This results in an increased expressive generator power, leading to a faster convergence towards the gate decomposition of  $U_T$  as we shall see below. Our proposal for learning  $U_T$  with an ancilla-assisted generator means that the input state for both, generator and target, is simply the product state of the Choi maximally entangled state of  $2N$ -qubits with an ancillary qubit:  $|\Omega'\rangle = |\Omega\rangle \otimes |0\rangle_a$ , where for simplicity we initialize the ancilla in the state  $|0\rangle$  and use the subscript  $a$  to denote it. Explicitly:

$$|\Omega'\rangle = \frac{1}{\sqrt{d}} \left( \sum_{i=0}^{d-1} |i\rangle_A |i\rangle_B \right) \otimes |0\rangle_a, \quad (3)$$

As shown in Fig. 1(a), the ancilla's action is only relevant to the generator, but since the discriminator requires comparing the outputs of our black box target  $T$  and the generator  $G$ , the Hilbert space in both ends must coincide, so an untouched ancilla qubit is also passed together with the target output.

The fidelity between the target and the generator output states is given now by:

$$F = |\langle \Omega' | (\mathbb{I}_A \otimes U_{Ga}^\dagger) (\mathbb{I}_A \otimes U_T \otimes \mathbb{I}_a) | \Omega' \rangle|^2 = \frac{1}{d^2} \left| \text{Tr}[U_G^\dagger U_T] \right|^2, \quad (4)$$

where now  $U_{Ga}$  is the unitary operator acting on half of the maximally entangled state plus the ancilla, as depicted in Fig. 1(c), and  $U_G' \equiv {}_a\langle 0 | U_{Ga} | 0 \rangle_a$  is its projection onto the ancillary subspace where the ancilla remains unchanged. As previously, high values of the fidelity correspond, up to a global phase, to  $U_G' \simeq U_T$ . Or equivalently  $U_{Ga} \simeq U_T \otimes |0\rangle_a\langle 0| \oplus V \otimes |1\rangle_a\langle 1|$ , with  $V$  being a redundant unitary. Therefore, even though on each layer of the generator, the ancilla interacts with the other qubits, the learning process leads  $U_{Ga}$  to a block diagonal form in the ancilla subspace, with  $U_T$  in one of the blocks, as shown schematically in Fig. 1(c).

In what follows, we demonstrate how the learning process is enhanced through the ancilla-assisted training. Specifically, we discuss in detail why the introduction of the ancilla during training can help to overcome stagnation. In essence, adding an ancilla at mid-training increases the dimensionality of the system dynamically, altering the cost function landscape and potentially opening up new optimization pathways, helping training escape local minima and plateaus.

As a proof of concept, we consider a simple 3-local target Hamiltonian,  $H_T = \sigma_z^1 \sigma_z^2 \sigma_z^3$ , with the corresponding operator,  $U_T = e^{-i\sigma_z^1 \sigma_z^2 \sigma_z^3}$ , acting on three qubits for a unit time. We remark that the specific choice of target does not impact the generality of the learning procedure presented here. As already pointed out, the generator consists of multiple layers, each with nearest-neighbor interactions and local rotations, as illustrated in Fig. 1(b), while the discriminator consists of a generalized local measurement, parametrized by a linear combination of Pauli operators, before a local computational basis measurement in each qubit. Both the discriminator and generator parameters are randomly initialized at the start of each training. This generator architecture becomes universal in the limit of infinitely many layers, as shown in Ref. [44]. Consequently, the expressivity of our generator increases with the number of layers. Based on our numerical results, the shorter gate sequence that performed sufficiently well is obtained using three layers. We fix this configuration for the remainder of our study.

Each training sequence will consist of up to 3000 iterations (6000 in total when two training are done sequentially, such as when an ancilla is added mid-training), or until a target fidelity of 99% is reached in iteration  $i^*$ , i.e.  $F_{i^*}^{(j)} \geq 0.99$ , where  $F_i^{(j)}$  denotes the fidelity in iteration  $i$  for the  $j$ th training run. For each run, we take as a figure of merit the maximum fidelity attained during training,  $F_{\max}^{(j)} = \max_i F_i^{(j)}$ . When multiple independent runs are performed, we report the average value of this same quantity:

$$F_{\max}^{\text{avg}} = \langle F_{\max}^{(j)} \rangle_j = \left\langle \max_i F_i^{(j)} \right\rangle_j.$$

With this, we analyze the impact of the ancillary qubit from three complementary perspectives: (i) its connectivity with the generator qubits, (ii) the timing of its introduction, and (iii) its initial parameters.

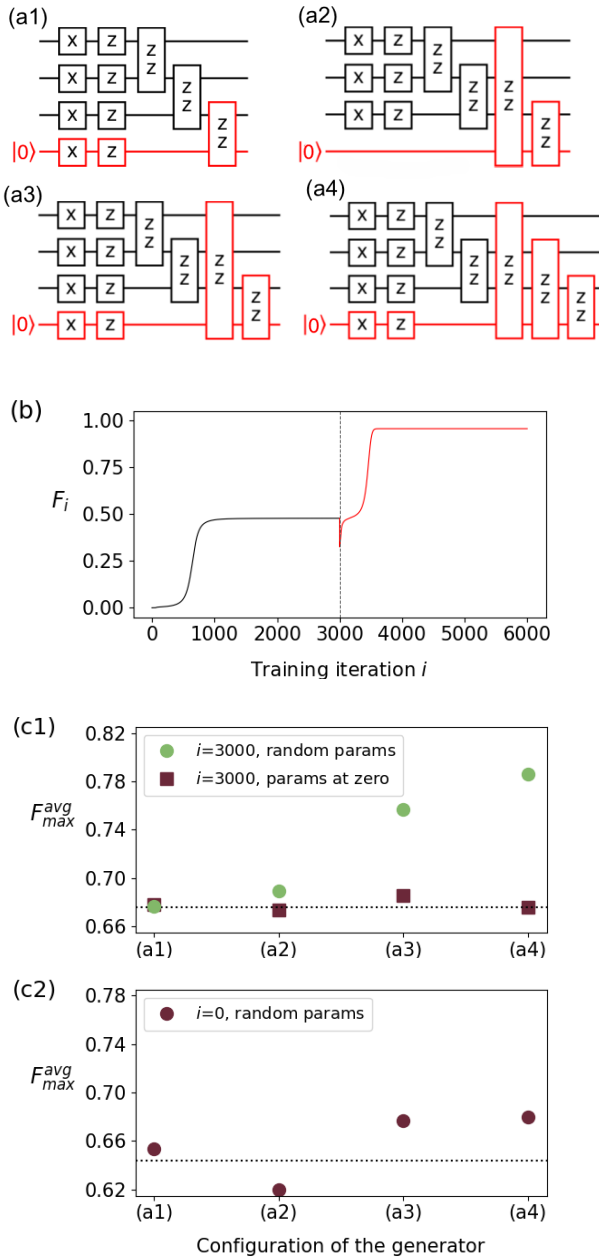


FIG. 2. Ancilla-assisted learning when the time evolution operator,  $e^{-i\sigma_z^1\sigma_z^2\sigma_z^3}$ , is generated with a hardware-efficient ansatz. (a) Ancilla configurations for each layer. (b) Fidelity  $F_i$  versus training iteration. In a typical run, a learning plateau is signalled by a fidelity saturating at  $F_i \ll 1$ . The plateau is overcome after adding an ancilla at iteration  $i = 3000$  (vertical dashed line) and letting the learning proceed. (c) The average maximum fidelity,  $F_{\max}^{\text{avg}}$ , is plotted against the ancilla configurations. The dotted horizontal line indicates the reference fidelity achieved in the absence of an ancilla. (c1) Ancilla is added in the middle of training. The green dots (brown squares) denote the fidelity when the parameters of the ancilla are initiated randomly (set to zero). (c2) Ancilla is added from the beginning of training with random initial parameters.

To explore the first crucial aspect, we consider several connectivity configurations for each layer, as shown in Fig. 2(a): (a1) the ancilla interacts with a single qubit; (a2/a3) the ancilla interacts with two qubits at the edges (without/with ancilla single qubit rotations); and (a4) the ancilla interacts with all generator qubits.

The timing at which the ancilla is introduced also strongly influences the learning process. We examine two scenarios: in the first, the ancilla is present from the start of training ( $i = 0$ ); in the second, it is added midway through the training ( $i = 3000$ ). In Fig. 2(b), we depict the average fidelity  $F_i$  versus the iteration for a typical run when the ancilla is added mid-training; where the initial training stagnates after a few iterations, and the fidelity reaches a steady value around  $F \simeq 0.5$ . Increasing the number of iterations does not improve the maximum fidelity, signaling stagnation. Finally, this is overcome by adding an ancilla in the middle of training with random initial parameters and connectivity (a3).

Following this, the last crucial aspect is randomizing the initial parameters of the ancilla to effectively use the increased optimization landscape. Randomization produces a “kick” to the system, which makes it jump out of the stagnation. Conversely, when the ancilla parameters are initially set to zero (no initial rotation), only marginal improvements are observed in Fig. 2(c1), indicating that a nontrivial initialization—or “kick”—is essential. Although note that randomization alone is not enough, when some parameters are randomized without expanding the phase space with an ancillary qubit, no improvement is achieved, as analyzed in Appendix A.

Therefore, for entanglement-assistance to be useful, the ancilla, together with its increase of the optimization landscape, should be introduced when stagnation has already occurred, and with a certain degree of randomness.

Our numerical results confirm such a description. When the ancilla is added at the start of the training ( $i = 0$ ), the improvement in fidelity is practically irrelevant ( $\leq 3\%$ ), irrespective of the connectivity of the ancillary qubit (a1-a4), as shown in Fig. 2(c2). On the other hand, clear improvement is observed in Fig. 2(c1), when the ancilla is added in the middle of the training process ( $i = 3000$ ), with randomized parameters. In this case, the average maximum fidelity increases by over 11% of its original value when the ancilla is connected to all qubits (a4), although fidelity also increases substantially ( $> 8.5\%$ ) when connected only to two previously unconnected qubits (a3), which points to an efficient implementation in current limited connectivities.

The reason for the improvements with these concrete connectivities can be demonstrated analytically by a dimensional expressivity analysis of the generator [45]. This is done by computing the Jacobian matrix of the circuit with respect to its parameters and examining its rank. As shown in Appendix B, the Jacobian rank of the circuit is highest for (a-4) and (a-3), indicating that they are the most expressive of our ancillary expansions.

*Summary.*— A major obstacle in quantum machine learning, and in variational quantum algorithms more broadly, is the emergence of learning plateaus and local minima in the optimization landscape, which severely hinders efficient training. These are particularly problematic when learning complex target unitaries using restricted generator models, as the expressivity gap often gives rise to vanishing gradients and poor convergence. Motivated by the need for practical strategies that alleviate stagnation without substantially increasing circuit depth or parameter count, we explore ancilla-assisted learning as a means to dynamically reshape the optimization landscape while preserving a realistic circuit-based implementation.

We have shown that introducing an ancilla qubit can significantly enhance learning performance when learning a target unitary  $U_T$  with a simpler generator  $U_G$ . Three features are critical to this improvement: entanglement between the ancilla and generator qubits, random initialization of the ancilla, and insertion of the ancilla at an intermediate epoch of the training process rather than at the start. Together, these ingredients increase the effective dimensionality of the Hilbert space and modify the geometry of the cost-function landscape favorably, enabling the optimizer to escape regions associated with learning plateaus and local minima. Numerical simulations confirm that this entanglement-assisted strategy markedly improves the approximation of a 3-local Hamiltonian using a 2-local generator, demonstrating that the approach can compensate for expressivity limitations in the model.

Although our numerical studies are restricted to small system sizes, the underlying mechanism- namely, the enlargement and restructuring of the accessible state space- suggests that ancilla-assisted learning may become even more powerful in larger-scale settings. In particular, the increased connectivity an ancilla can bring to larger systems, with more distant qubits, is expected to further enhance expressivity and gradient flow. The protocol's reliance on random initialization and timed ancilla insertion also points toward more general strategies for dynamically varying the ansatz during training. These ideas could be integrated with other techniques, such as adaptive circuit growth [46, 47] or noise-aware training [48], and may be relevant also in variational quantum simulation [49] and quantum control [50].

Several important questions remain open. First, how the benefits of ancilla assistance scale with system size, circuit depth, and noise, in realistic hardware implementations needs further exploration. Second, the optimal timing and number of ancilla qubits required for different learning tasks have yet to be systematically characterized. Third, a deeper theoretical understanding of how ancilla-induced entanglement reshapes the cost-function landscape and affects gradient statistics would be valuable. Addressing these questions will be essential for determining whether ancilla-assisted strategies provide scalable solutions to learning plateaus

in practical quantum machine learning applications.

*Acknowledgments.*— We acknowledge stimulating discussions with María García Díaz and Mohammad Mehboudi. A.U. is financially supported by JSPS Overseas Research Fellowships. G.A.L. acknowledges support from the program of predoctoral funds FISTEP (2025-3XJ3GQYK8), from Departament de Recerca i Universitats of Generalitat de Catalunya, and the co-financing by Fons Social Europeu Plus. We acknowledge support from MICINN grant PID2022-139099NBI00, with the support of FEDER funds, the Spanish Government with funding from European Union NextGenerationEU (PRTR-C17.II), the Generalitat de Catalunya, the Ministry for Digital Transformation and of Civil Service of the Spanish Government through the QUANTUM ENIA project -Quantum Spain Project- through the Recovery, Transformation and Resilience Plan NextGeneration EU within the framework of the Digital Spain 2026.

*Data availability.*— The code used for this work is available online [51].

## REFERENCES

- [1] T. Olsacher, T. Kraft, C. Kokail, B. Kraus, and P. Zoller, Hamiltonian and liouvillian learning in weakly-dissipative quantum many-body systems, *Quantum Science and Technology* **10**, 015065 (2025).
- [2] N. Wiebe, C. Granade, C. Ferrie, and D. G. Cory, Hamiltonian learning and certification using quantum resources, *Phys. Rev. Lett.* **112**, 190501 (2014).
- [3] J. Wang, S. Paesani, R. Santagati, S. Knauer, A. A. Gentile, N. Wiebe, M. Petruzzella, J. L. O'Brien, J. G. Rarity, A. Laing, and M. G. Thompson, Experimental quantum hamiltonian learning, *Nature Physics* **13**, 551–555 (2017).
- [4] E. Bairey, I. Arad, and N. H. Lindner, Learning a local hamiltonian from local measurements, *Phys. Rev. Lett.* **122**, 020504 (2019).
- [5] Z. Li, L. Zou, and T. H. Hsieh, Hamiltonian tomography via quantum quench, *Phys. Rev. Lett.* **124**, 160502 (2020).
- [6] S.-T. Wang, D.-L. Deng, and L.-M. Duan, Hamiltonian tomography for quantum many-body systems with arbitrary couplings, *New Journal of Physics* **17**, 093017 (2015).
- [7] P. Bienias, A. Seif, and M. Hafezi, *Meta hamiltonian learning* (2021), arXiv:2104.04453 [quant-ph].
- [8] D. Hangleiter, I. Roth, J. Fuksa, J. Eisert, and P. Roushan, *Robustly learning the hamiltonian dynamics of a superconducting quantum processor* (2024), arXiv:2108.08319 [quant-ph].
- [9] A. Zubida, E. Yitzhaki, N. H. Lindner, and E. Bairey, *Optimal short-time measurements for hamiltonian learning* (2021), arXiv:2108.08824 [quant-ph].
- [10] W. Yu, J. Sun, Z. Han, and X. Yuan, Robust and Efficient Hamiltonian Learning, *Quantum* **7**, 1045 (2023).
- [11] L. Pastori, T. Olsacher, C. Kokail, and P. Zoller, Characterization and verification of trotterized digital quantum

simulation via hamiltonian and liouvillian learning, *PRX Quantum* **3**, 030324 (2022).

[12] A. Zhao, Learning the structure of any hamiltonian from minimal assumptions, in *Proceedings of the 57th Annual ACM Symposium on Theory of Computing*, STOC '25 (Association for Computing Machinery, New York, NY, USA, 2025) p. 1201–1211.

[13] S. Arunachalam, A. Dutt, and F. E. Gutiérrez, *Testing and learning structured quantum hamiltonians* (2025), arXiv:2411.00082 [quant-ph].

[14] H.-Y. Hu, M. Ma, W. Gong, Q. Ye, Y. Tong, S. T. Flammia, and S. F. Yelin, Ansatz-free hamiltonian learning with heisenberg-limited scaling, *PRX Quantum* **6**, 040315 (2025).

[15] X.-L. Qi and D. Ranard, Determining a local Hamiltonian from a single eigenstate, *Quantum* **3**, 159 (2019).

[16] R. P. Feynman, Simulating physics with computers, *International Journal of Theoretical Physics* **21**, 467 (1982).

[17] S. Lloyd, Universal quantum simulators, *Science* **273**, 1073 (1996).

[18] E. Altman, K. R. Brown, G. Carleo, L. D. Carr, E. Demler, C. Chin, B. DeMarco, S. E. Economou, M. A. Eriksson, K.-M. C. Fu, M. Greiner, K. R. Hazzard, R. G. Hulet, A. J. Kollár, B. L. Lev, M. D. Lukin, R. Ma, X. Mi, S. Misra, C. Monroe, K. Murch, Z. Nazario, K.-K. Ni, A. C. Potter, P. Roushan, M. Saffman, M. Schleier-Smith, I. Siddiqi, R. Simmonds, M. Singh, I. Spielman, K. Temme, D. S. Weiss, J. Vučković, V. Vuletić, J. Ye, and M. Zwierlein, Quantum simulators: Architectures and opportunities, *PRX Quantum* **2**, 017003 (2021).

[19] A. J. Daley, I. Bloch, C. Kokail, S. Flannigan, N. Pearson, M. Troyer, and P. Zoller, Practical quantum advantage in quantum simulation, *Nature* **607**, 667 (2022).

[20] M. E. Beverland, P. Murali, M. Troyer, K. M. Svore, T. Hoefler, V. Kliuchnikov, G. H. Low, M. Soeken, A. Sundaram, and A. Vaschillo, Assessing requirements to scale to practical quantum advantage (2022), arXiv:2211.07629 [quant-ph].

[21] T. S. Cubitt, A. Montanaro, and S. Piddock, Universal quantum hamiltonians, *Proceedings of the National Academy of Sciences* **115**, 9497 (2018), <https://www.pnas.org/doi/pdf/10.1073/pnas.1804949115>.

[22] A. Usui, A. Sanpera, and M. García Díaz, Simplifying the simulation of local hamiltonian dynamics, *Phys. Rev. Res.* **6**, 023243 (2024).

[23] W. Gong, S. Zhou, and T. Li, Complexity of Digital Quantum Simulation in the Low-Energy Subspace: Applications and a Lower Bound, *Quantum* **8**, 1409 (2024).

[24] S. Lloyd and C. Weedbrook, Quantum generative adversarial learning, *Phys. Rev. Lett.* **121**, 040502 (2018).

[25] P.-L. Dallaire-Demers and N. Killoran, Quantum generative adversarial networks, *Phys. Rev. A* **98**, 012324 (2018).

[26] I. J. Goodfellow, J. Pouget-Abadie, M. Mirza, B. Xu, D. Warde-Farley, S. Ozair, A. Courville, and Y. Bengio, Generative adversarial nets, *Advances in neural information processing systems* **27** (2014).

[27] L. Hu, S.-H. Wu, W. Cai, Y. Ma, X. Mu, Y. Xu, H. Wang, Y. Song, D.-L. Deng, C.-L. Zou, and L. Sun, Quantum generative adversarial learning in a superconducting quantum circuit, *Science Advances* **5**, 10.1126/sciadv.aav2761 (2019).

[28] K. Huang, Z.-A. Wang, C. Song, K. Xu, H. Li, Z. Wang, Q. Guo, Z. Song, Z.-B. Liu, D. Zheng, D.-L. Deng, H. Wang, J.-G. Tian, and H. Fan, Quantum generative adversarial networks with multiple superconducting qubits, *npj Quantum Information* **7**, 165 (2021).

[29] S. Ahmed, C. Sánchez Muñoz, F. Nori, and A. F. Kockum, Quantum state tomography with conditional generative adversarial networks, *Physical Review Letters* **127**, 10.1103/physrevlett.127.140502 (2021).

[30] C. Zoufal, A. Lucchi, and S. Woerner, Quantum generative adversarial networks for learning and loading random distributions, *npj Quantum Information* **5**, 10.1038/s41534-019-0223-2 (2019).

[31] M. Benedetti, E. Grant, L. Wossnig, and S. Severini, Adversarial quantum circuit learning for pure state approximation, *New Journal of Physics* **21**, 043023 (2019).

[32] H.-L. Huang, Y. Du, M. Gong, Y. Zhao, Y. Wu, C. Wang, S. Li, F. Liang, J. Lin, Y. Xu, R. Yang, T. Liu, M.-H. Hsieh, H. Deng, H. Rong, C.-Z. Peng, C.-Y. Lu, Y.-A. Chen, D. Tao, X. Zhu, and J.-W. Pan, Experimental quantum generative adversarial networks for image generation, *Physical Review Applied* **16**, 10.1103/physrevapplied.16.024051 (2021).

[33] S. A. Stein, B. Baheri, D. Chen, Y. Mao, Q. Guan, A. Li, B. Fang, and S. Xu, Qugan: A quantum state fidelity based generative adversarial network, in *2021 IEEE International Conference on Quantum Computing and Engineering (QCE)* (IEEE, 2021) p. 71–81.

[34] S. Chakrabarti, Y. Huang, T. Li, S. Feizi, and X. Wu, *Quantum wasserstein generative adversarial networks* (2019), arXiv:1911.00111 [quant-ph].

[35] T. A. Ngo, T. Nguyen, and T. C. Thang, A survey of recent advances in quantum generative adversarial networks, *Electronics* **12**, 10.3390/electronics12040856 (2023).

[36] L. Kim, S. Lloyd, and M. Marvian, Hamiltonian quantum generative adversarial networks, *Phys. Rev. Res.* **6**, 033019 (2024).

[37] G. De Palma, M. Marvian, D. Trevisan, and S. Lloyd, The quantum wasserstein distance of order 1, *IEEE Transactions on Information Theory* **67**, 6627 (2021).

[38] B. T. Kiani, G. De Palma, M. Marvian, Z.-W. Liu, and S. Lloyd, Learning quantum data with the quantum earth mover's distance, *Quantum Science and Technology* **7**, 045002 (2022).

[39] M.-D. Choi, Completely positive linear maps on complex matrices, *Linear Algebra and its Applications* **10**, 285 (1975).

[40] A. Jamiołkowski, Linear transformations which preserve trace and positive semidefiniteness of operators, *Reports on Mathematical Physics* **3**, 275 (1972).

[41] H.-L. Huang, Y. Du, M. Gong, Y. Zhao, Y. Wu, C. Wang, S. Li, F. Liang, J. Lin, Y. Xu, R. Yang, T. Liu, M.-H. Hsieh, H. Deng, H. Rong, C.-Z. Peng, C.-Y. Lu, Y.-A. Chen, D. Tao, X. Zhu, and J.-W. Pan, Experimental quantum generative adversarial networks for image generation, *Physical Review Applied* **16**, 10.1103/physrevapplied.16.024051 (2021).

[42] J. R. McClean, S. Boixo, V. N. Smelyanskiy, R. Babbush, and H. Neven, Barren plateaus in quantum neural network training landscapes, *Nature Communications* **9**, 10.1038/s41467-018-07090-4 (2018).

[43] E. R. Anschuetz and B. T. Kiani, Quantum variational algorithms are swamped with traps, *Nature Communications* **13**, 10.1038/s41467-022-35364-5 (2022).

- [44] A. Barenco, C. H. Bennett, R. Cleve, D. P. DiVincenzo, N. Margolus, P. Shor, T. Sleator, J. A. Smolin, and H. Weinfurter, Elementary gates for quantum computation, *Phys. Rev. A* **52**, 3457 (1995).
- [45] L. Funcke, T. Hartung, K. Jansen, S. Kühn, and P. Stornati, Dimensional Expressivity Analysis of Parametric Quantum Circuits, *Quantum* **5**, 422 (2021).
- [46] H. R. Grimsley, S. E. Economou, E. Barnes, and N. J. Mayhall, An adaptive variational algorithm for exact molecular simulations on a quantum computer, *Nature Communications* **10**, 3007 (2019).
- [47] H. L. Tang, V. Shkolnikov, G. S. Barron, H. R. Grimsley, N. J. Mayhall, E. Barnes, and S. E. Economou, Qubit-adapt-vqe: An adaptive algorithm for constructing hardware-efficient ansätze on a quantum processor, *PRX Quantum* **2**, 020310 (2021).
- [48] H. Wang, J. Gu, Y. Ding, Z. Li, F. T. Chong, D. Z. Pan, and S. Han, Quantumnat: quantum noise-aware training with noise injection, quantization and normalization, in *Proceedings of the 59th ACM/IEEE Design Automation Conference*, DAC '22 (Association for Computing Machinery, New York, NY, USA, 2022) p. 1–6.
- [49] X. Yuan, S. Endo, Q. Zhao, Y. Li, and S. C. Benjamin, Theory of variational quantum simulation, *Quantum* **3**, 191 (2019).
- [50] R. de Keijzer, O. Tse, and S. Kokkelmans, Pulse based Variational Quantum Optimal Control for hybrid quantum computing, *Quantum* **7**, 908 (2023).
- [51] A. Usui and G. Abad López, [https://github.com/ayaka-usui/qgan\\_subspace](https://github.com/ayaka-usui/qgan_subspace) (2025).
- [52] D. J. Egger, J. Mareček, and S. Woerner, Warm-starting quantum optimization, *Quantum* **5**, 479 (2021).
- [53] M. Kashif and M. Shafique, The dilemma of random parameter initialization and barren plateaus in variational quantum algorithms (2024), arXiv:2412.06462 [quant-ph].

## SUPPLEMENTAL MATERIAL

### Appendix A: Randomised restart

In the main text, we study the impact of an ancilla on the efficiency of the learning process. Particularly, we found that adding an ancilla in the middle of training makes the learning efficient and that the parameters involved with the ancilla are more effective when randomized than when initialized to zero. Here, we study another possible approach without using additional qubits in comparison and consider randomizing some of the parameters of the generator. Specifically, in the middle of training, we choose some of the parameters randomly at some ratio and replace them with random numbers. This can be regarded as restarting the training with some prior information. A question is whether such prior information speeds up the learning and whether kicking the generator in this way overcomes the ancilla case. We find that this is not the case, as demonstrated below. Fig. 3 shows the averaged maximum fidelities for different ratios we choose for randomization. Large deviation from the case where the parameters are not modified through the training is not observed.

This approach is inspired by “warm start” [52, 53], where one selects initial points convenient to reach high fidelity. In our case, we select the parameters for the second 3000 iteration routine based on those for the first 3000 iteration routine. In comparison with when the parameters are chosen fully randomly, our case sets parameters “close” to reach a high value of the fidelity.

The selection of parameters to be changed in the middle of training is critical. In our case, we select them randomly and find that it does not work well. If prior information is constructed more informedly, it may work better, and more investigation is needed for this.

Nevertheless, it is clear that, compared to this result, the advantage obtained by adding the ancilla comes from

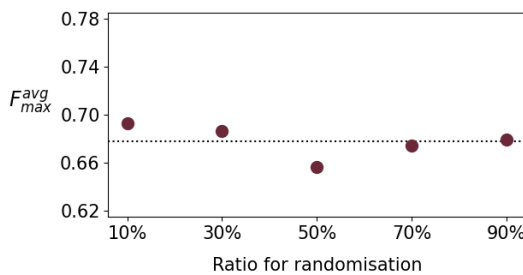


FIG. 3. Randomised restart approach, when the time evolution operator  $e^{-i\sigma_z^1\sigma_z^2\sigma_z^3}$  is targeted. Maximum reached fidelity ( $F_{max}^{avg}$ ), given by Eq. (2), averaged over 100 attempts, for different randomization ratios we choose. The generator is trained first for 3000 iterations, and then after some of the parameters are randomized, for another 3000 iterations. The dotted lines represent the reference fidelity achieved when no randomization is done.

the fact that the dimensions of the system are expanded and not just that some of the parameters are randomized.

### Appendix B: Expressivity Analysis

We have shown that the performance of QGAN depends on the connectivity configuration of the ancilla, and a configuration that connects distant qubits of the generator improves the learning. In this section, we give an analytical explanation for this using the dimensional expressivity analysis introduced in Ref. [45].

Dimensional expressivity analysis allows us to determine the number of independent circuit parameters, and hence, a circuit that has a higher expressivity will have fewer redundant parameters. By computing the Jacobian matrix of the circuit, we determine the dimension of the manifold of states that is accessible to the circuit. If the rank equals the number of parameters, all the parameters independently expand the reachable state space; if not, some of the parameters are redundant because they do not change the output state in a new direction.

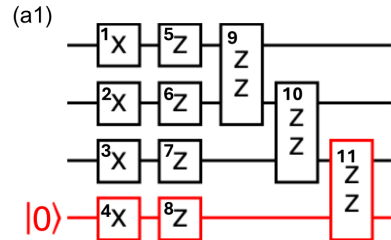


FIG. 4. Expressivity analysis of the ancilla-assisted learning protocol. Optimization of expressivity corresponds to a larger rank of the Jacobian (see B1). In the figure, we enumerate the parameters corresponding to the circuit C(a-1). Other circuits (C(a-2) – C(a-4)) are treated similarly.

We now apply this analysis to the circuit configurations given in Fig. 2(a). Configuration a2 can be viewed as a special case of a3, obtained by setting the ancilla’s local rotations to zero. Since this does not generate any new interaction between the ancilla and the generator qubits, we restrict our attention to configurations a1, a3, and a4.

Let us denote the circuit corresponding to the configuration-(an) with  $N$  parameters  $\theta = (\theta_1, \dots, \theta_N)$  as  $C_n(\theta)$ , where  $n = 1, 3, 4$ . For convenience, we drop the notation  $\theta$  for the remainder of this manuscript. We define the Jacobian of the circuit as

$$J_n(\theta) = \begin{pmatrix} \frac{\partial C_n}{\partial \theta_1}(\theta) & \frac{\partial C_n}{\partial \theta_2}(\theta) & \dots & \frac{\partial C_n}{\partial \theta_N}(\theta) \end{pmatrix}. \quad (B1)$$

The expressivity of  $C_n$  is defined as  $\mathcal{E}_n := \text{rank}(J_n(\theta))$ . Physically, it denotes the manifold of quantum states reachable by the circuit.

**Proposition 1** Consider the circuit  $C_n$  corresponding to the configuration-(an) for  $n = 1, 3, 4$ . Then, the expressivity of the circuits follows the ordering  $\mathcal{E}_4 > \mathcal{E}_3 > \mathcal{E}_1$  whenever the parameters are not zero.

**Proof.** We start by observing that  $C_3 = e^{-i\frac{\Phi}{2}\sigma_z^1\sigma_z^4}C_1$ . Hence, for any range of parameters of  $C_1$ ,  $C_3$  can achieve the same expressivity by setting  $\Phi = 0$ , demonstrating that  $\mathcal{E}_3 \geq \mathcal{E}_1$ . Observing that  $C_4 = e^{-i\frac{\Theta}{2}\sigma_z^1\sigma_z^3}C_3$  and

applying the same reasoning, we obtain  $\mathcal{E}_4 \geq \mathcal{E}_3 \geq \mathcal{E}_1$ .

We now establish the strict inequality numerically. To do this, we randomly sample parameters for each circuit and calculate the corresponding expressivity using Eq. (B1). For completeness, we shall describe how the analysis is performed for  $C_1$ . The calculations for the other circuits follow in a similar manner. Let us define the unitaries,

$$U_{\text{ent}} = (I \otimes I \otimes R_{ZZ}(\theta_{11})) (I \otimes R_{ZZ}(\theta_{10}) \otimes I) (R_{ZZ}(\theta_9) \otimes I \otimes I), \quad (\text{B2})$$

$$U_0 = (R_z(\theta_5) R_x(\theta_1)) \otimes (R_z(\theta_6) R_x(\theta_2)) \otimes (R_z(\theta_7) R_x(\theta_3)) \otimes (R_z(\theta_8) R_x(\theta_4)). \quad (\text{B3})$$

Now we write  $C_1 = U_{\text{ent}} U_0$ . Let us enumerate the eleven circuit parameters as shown in Fig. 4. The partial derivative of  $C_1$  with respect to  $\theta_k$  is denoted as  $\partial(\theta_k)$ .

$$\begin{aligned} \partial(\theta_1) &= -\frac{i}{2} U_{\text{ent}} (X \otimes I \otimes I \otimes I) U_0 |0000\rangle, \\ \partial(\theta_2) &= -\frac{i}{2} U_{\text{ent}} (I \otimes X \otimes I \otimes I) U_0 |0000\rangle, \\ \partial(\theta_3) &= -\frac{i}{2} U_{\text{ent}} (I \otimes I \otimes X \otimes I) U_0 |0000\rangle, \\ \partial(\theta_4) &= -\frac{i}{2} U_{\text{ent}} (I \otimes I \otimes I \otimes X) U_0 |0000\rangle, \\ \partial(\theta_5) &= -\frac{i}{2} U_{\text{ent}} (Z \otimes I \otimes I \otimes I) U_0 |0000\rangle, \\ \partial(\theta_6) &= -\frac{i}{2} U_{\text{ent}} (I \otimes Z \otimes I \otimes I) U_0 |0000\rangle, \\ \partial(\theta_7) &= -\frac{i}{2} U_{\text{ent}} (I \otimes I \otimes Z \otimes I) U_0 |0000\rangle, \\ \partial(\theta_8) &= -\frac{i}{2} U_{\text{ent}} (I \otimes I \otimes I \otimes Z) U_0 |0000\rangle, \\ \partial(\theta_9) &= -\frac{i}{2} ((Z \otimes Z) \otimes I \otimes I) U_{\text{ent}} U_0 |0000\rangle, \\ \partial(\theta_{10}) &= -\frac{i}{2} (I \otimes (Z \otimes Z) \otimes I) U_{\text{ent}} U_0 |0000\rangle, \\ \partial(\theta_{11}) &= -\frac{i}{2} (I \otimes I \otimes (Z \otimes Z)) U_{\text{ent}} U_0 |0000\rangle. \end{aligned}$$

We sample  $10^6$  random values for the parameters

$\theta_1, \theta_2, \dots, \theta_{11}$  and calculate the expressivity. We do the same for  $C_3$  and  $C_4$ , each having twelve and thirteen parameters, respectively. When the parameters are not equal to zero, we find that the expressivities satisfy the inequality  $\mathcal{E}_4 > \mathcal{E}_3 > \mathcal{E}_1$ . However, all the circuits have the same expressivity when the parameters are set to zero. This completes the proof.  $\blacksquare$

In the main text, we see a significant improvement in learning performance when going from (a1) to (a3) and then to (a4). Proposition 1 gives a rigorous theoretical explanation for this phenomenon. In configuration (a1), the ancilla interacts with a single qubit of the generator, whereas in (a2), it interacts with two qubits that are not linked by any gates. Thus, (a2) creates a mediated channel for entangling two distant qubits. However, (a2) does not have local rotations on the ancilla, and this is rectified in (a3), for which we see a significant increase in  $F_{\text{max}}^{\text{avg}}$ . This is taken a step further in (a4), where the ancilla interacts with all the qubits, and we see improved performance. How to choose a configuration for a given Hamiltonian is an interesting question to ask at this juncture. While (a4) gives the best fidelities, it requires an extra gate, which would be demanding to perform in a lab. On the other hand, (a3) achieves a slightly lower fidelity with fewer resources. A precise cost-benefit analysis of the number of gates required and the fidelities achieved is required, which we leave for future work.